Periodic stripe domains and hybrid-alignment regime in nematic liquid crystals: Threshold analysis

A. Sparavigna,[1] O. D. Lavrentovich,[2,*] and A. Strigazzi[1]
[1]*Dipartimento di Fisica, Politecnico di Torino, Corso Duca degli Abruzzi 24, I-10129, Torino, Italy*
[2]*Liquid Crystal Institute and Physics Department, Kent State University, Kent, Ohio 44242*
(Received 14 July 1993)

Recently we investigated the occurrence of static periodic stripes in a hybrid aligned nematic cell. Assuming that the tilt anchoring was stronger at the planar wall than at the homeotropic wall, we have found the critical thickness of the cell for the transition from planar to periodic alignment as a function of the surface energy in the presence of a magnetic field. Here we study, for the same kind of cell, the critical thickness between the periodic and the aperiodic deformed structure by means of an appropriate numerical technique. As expected, such a threshold was found to be greater than the asymptotic threshold between planar and aperiodic structures. We performed an experiment, which allowed us to give an estimate of the surfacelike elastic constant K_{24}.

PACS number(s): 61.30.Gd, 68.10.Cr

I. INTRODUCTION

In recent papers [1–4] the occurrence of static periodic stripes in the hybrid aligned nematic layers has been investigated. Such cells possess homeotropic (*H*) anchoring at one of the walls and unidirectional planar anchoring (*P*) at the other [5]; moreover, the planar anchoring was assumed to be stronger than the homeotropic one. In this kind of cell, three different behaviors of the director (that is, of the local mean orientation of the molecules) can occur. Since the *P* anchoring is the stronger one, the director can assume a uniform distribution parallel to the easy direction of the planar wall (*P*) when the thickness d is lower than a critical one; above such a value, an aperiodic deformed hybrid alignment of the nematic cell (HAN) and a periodic deformed structure (PHAN) can be achieved (see Fig. 1). The periodic pattern in *P*-oriented nematics was earlier discussed by Bobylev and Pikin [6] as due to a flexoelectric coupling with an imposed electric field: later, it was observed by Lonberg and Meyer in the case of strong anchoring [7] and studied by Miraldi, Oldano, and Strigazzi in *P*-nematic layers weakly anchored in the presence of an external magnetic field [8]. Only recently, the occurrence of the PHAN structure in a hybrid cell without external field has been discovered: in this case, the role of the field is formally played by the cell thickness, but the real cause of the instability is the nonzero saddle-splay rigidity of the nematic [9,10]. Our previous papers on this subject have been devoted to the analysis of the transition between the PHAN and the *P* configuration. We studied [1,2] the dependency of the threshold thickness, that is, of the cell thickness above which the PHAN is allowed, on the elastic constants and on the anchoring strengths [11]. Furthermore, we also considered the influence on this threshold of a magnetic field normal to the cell plates [3,4].

When the possibility of the existence of a PHAN structure was not known, Barbero and Barberi [12] dealt with the *P*-HAN transition, and obtained the threshold dependency on the tilt anchoring strengths. The question now arises, where is the actual PHAN-HAN threshold? Is it maybe above the "asymptotic" *P*-HAN threshold found in Ref. [12]? Moreover, is the PHAN structure always possible? In the present paper we investigate these points, in the framework of a nonlinearized approach for a model treating nematics with bulk elastic isotropy ($K \equiv K_{11} = K_{22} = K_{33}$) in the absence of external fields. This simplified model is necessary since the theory for the PHAN-HAN transition is much more complex than the one for *P*-PHAN transition.

The aim of our work is to describe theoretically the PHAN-HAN transition and to compare the model with preliminary experimental data concerning the nematic liquid crystal pentylcyanobiphenyl (5CB), which allow an estimate of the saddle-splay elastic constant K_{24}.

II. THEORY

The distortion free-energy density of Nehring and Saupe [13], in the case of a nematic liquid crystal having bulk elastic isotropy, in the framework of the usual first-order continuum theory [14] is given by

$$f = \tfrac{1}{2}K\{(\mathrm{div}\mathbf{n})^2 + (\mathbf{n}\cdot\mathrm{curl}\mathbf{n})^2 + (\mathbf{n}\times\mathrm{curl}\mathbf{n})^2\} - (K + K_{24})\mathrm{div}[\mathbf{n}\cdot\mathrm{div}\mathbf{n} + \mathbf{n}\times\mathrm{curl}\mathbf{n}] , \quad (1)$$

where $K \equiv K_{11} = K_{22} = K_{33}$ is the common bulk elastic constant, K_{24} is the saddle-splay elastic constant, and $\mathbf{n}$ is the nematic director, i.e., the local average of the molecular long axis. Let us assume a Cartesian reference frame $[xyz]$, $[xy]$ being the plane coincident with the *H* wall $z_0 = 0$, where the easy direction is homeotropic, whereas z is the coordinate normal to the substrates. Then the oth-

*Also with Institute of Physics, Academy of Science of Ukraine, Kiev-28, Ukraine.

er wall, where the easy direction is unidirectional and planar, is identified by $z_1=d$, d being the cell thickness. Moreover, at the P substrate the easy direction is parallel to the x axis.

The director $\mathbf{n}$ may be described by two angles in a polar reference frame $[\phi,\theta]$, where the azimuth ϕ is accounted for in the plane $[xy]$ from the x axis, while the polar angle θ is measured out of the plane $[xy]$. Hence

$$\mathbf{n}=\mathbf{i}\cos\phi\cos\theta+\mathbf{j}\sin\phi\cos\theta+\mathbf{k}\sin\theta\ . \tag{2}$$

For the P-PHAN transition, we can expand to the second power the reduced free-energy density $g=2f/K$ around the undeformed planar structure $(\theta=0,\phi=0)$ [2], obtaining the parabolic contribution to the reduced free-energy density actually confined to the bulk in the simple form

$$g_b=(\phi_y+\theta_z)^2+(\theta_y-\phi_z)^2\ , \tag{3}$$

where the subscripts y,z refer to the derivatives with respect to the corresponding coordinates.

In fact, the saddle-splay contribution g_{SS} goes to the surface, due to Gauss's theorem, giving rise to the second-order terms

$$g_{SS}=2(1+\kappa_4)[-\phi_0\theta_{y0}+\theta_0\phi_{y0}+\phi_1\theta_{y1}-\theta_1\phi_{y1}]\ , \tag{4}$$

where $\kappa_4\equiv K_{24}/K$ is the surface-to-bulk elastic ratio and the subscript $j=0,1$ refers to the $z_0=0$, $z_1=d$ substrates, respectively. Moreover, the azimuthal and tilt anchoring contributions, according to Rapini-Papoular [11], write to the second-order terms

$$g_w=L_{\phi 0}^{-1}\phi_0^2-L_{\theta 0}^{-1}\theta_0^2+L_{\phi 1}^{-1}\phi_1^2+L_{\theta 1}^{-1}\theta_1^2\ , \tag{5}$$

where $L_{\phi j}\equiv K/W_{\phi j}$, $L_{\theta j}\equiv K/W_{\theta j}$ are the de Gennes–Kléman extrapolation lengths [15,16], $W_{\phi j}, W_{\theta j}$ being the torsional and tilt anchoring strengths.

The reduced free energy G is then obtained as

$$\begin{aligned} &G=G_b+G_s\ ,\\ &G_b\equiv\int_0^\lambda dy\int_0^d g_b(\theta_y,\phi_y,\theta_z,\phi_z)dz\ ,\\ &G_s\equiv\int_0^\lambda g_s(\theta_j,\phi_j,\theta_{yj},\phi_{yj})dy\ ,\\ &g_s=g_{SS}+g_w\ , \end{aligned} \tag{6}$$

λ being the wavelength of the periodic pattern, whose wave vector $\beta\equiv 2\pi/\lambda$ is parallel to the y axis, i.e., transverse to the P easy direction. Close to the P-PHAN transition, g_b and g_s are expanded to the second power in the angles ϕ,θ.

Instead, if the PHAN-HAN transition is concerned, we have to work around the aperiodic deformed structure (HAN): due to this fact, it is only possible to linearize the torques on ϕ, θ being generally finite and different from zero.

Linearizing only on ϕ, we obtain a reduced free-energy density g_b actually confined to the bulk in the form

$$g_b=\theta_y^2+\theta_z^2+(\phi_y^2+\phi_z^2)\cos^2\theta+2(\phi_y\theta_z-\theta_y\phi_z)\cos^2\theta\ . \tag{3'}$$

The saddle splay becomes now

$$g_{SS}=2(1+\kappa_4)[-\phi_0\theta_{y0}+\tfrac{1}{2}\phi_{y0}\sin 2\theta_0+\phi_1\theta_{y1}-\tfrac{1}{2}\phi_{y1}\sin 2\theta_1]\ . \tag{4'}$$

On the other hand, implementing the Rapini-Papoular approach, the nonlinear anchoring energy density must be written in covariant form

$$f_W^j=[-a_j(\mathbf{n}\cdot\mathbf{i})^2+(-1)^{j+1}b_j(\mathbf{n}\cdot\mathbf{k})^2]\ ,\quad j=0,1\ , \tag{7}$$

where a_j and b_j are positive, and $a_0<b_0$. We stress the fact that at the H wall $(j=0)$ there is an easy plane, i.e.,

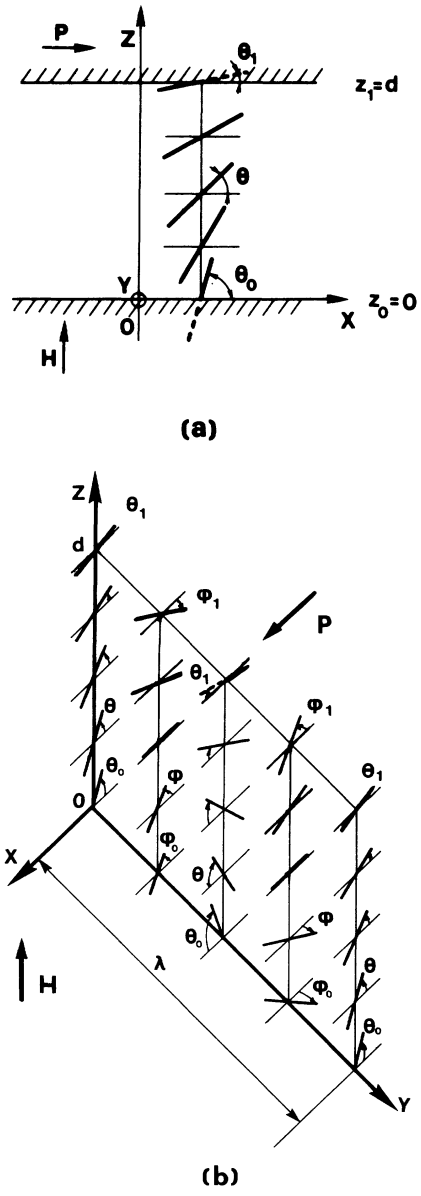

FIG. 1. (a) Aperiodic configuration in a hybrid aligned nematic (HAN) cell, having tilt anchoring weaker at the wall $z_0=0$, where the preferred direction is homeotropic (H), than at the wall $z_1=d$, where the easy direction is unidirectional planar (P); (b) Periodic hybrid aligned nematic (PHAN) cell of splay type: the leading parameter is the cell thickness d, which plays the role of an external field.

[xz], whereas at the P wall ($j=1$) the easy plane is the P wall itself. The tilt anchoring strengths $W_{\theta j}$ are derived by normalizing (7) for $\phi_j=0$, while the torsional anchoring strength $W_{\phi j}$ is normalized by applying to (7) the condition $\theta_j=0$. In fact we have

$$a_j=\tfrac{1}{2}W_{\phi j}\ ,$$
$$b_j=\tfrac{1}{2}(-1)^j(W_{\phi j}+W_{\theta j})\ . \tag{8}$$

Hence Eq. (7) finally reads

$$f_W^j=\tfrac{1}{2}[W_{\phi j}\sin^2\phi_j\cos^2\theta_j+(-1)^{j+1}W_{\theta j}\sin^2\theta_j] \tag{7'}$$

and the reduced anchoring energy density, linearized only on ϕ_j, is obtained as

$$g_W=L_{\phi 0}^{-1}\phi_0^2\cos^2\theta_0-L_{\theta 0}^{-1}\sin^2\theta_0 +L_{\phi 1}^{-1}\phi_1^2\cos^2\theta_1+L_{\theta 1}^{-1}\sin^2\theta_1\ . \tag{5'}$$

Following the usual procedure [17], we linearize only on ϕ the Euler-Lagrange equations

$$\frac{\partial g_b}{\partial\theta}=\frac{\partial}{\partial z}\frac{\partial g_b}{\partial\theta_z}+\frac{\partial}{\partial y}\frac{\partial g_b}{\partial\theta_y}\ ,$$
$$\frac{\partial g_b}{\partial\phi}=\frac{\partial}{\partial z}\frac{\partial g_b}{\partial\phi_z}+\frac{\partial}{\partial y}\frac{\partial g_b}{\partial\phi_y}\ , \tag{9}$$

and obtain

$$\theta_{zz}+\theta_{yy}=0\ ,$$
$$\phi_{zz}+\phi_{yy}-2\theta_z\phi_z\tan\theta=0\ . \tag{10}$$

Hence the boundary conditions

$$\left[\pm\frac{\partial g_b}{\partial\theta_z}+\frac{\partial g_s}{\partial\theta}-\frac{\partial}{\partial y}\frac{\partial g_s}{\partial\theta_y}\right]_0^1=0\ ,$$
$$\left[\pm\frac{\partial g_b}{\partial\phi_z}+\frac{\partial g_s}{\partial\phi}-\frac{\partial}{\partial y}\frac{\partial g_s}{\partial\phi_y}\right]_0^1=0\ , \tag{11}$$

in the same assumption read

$$\theta_{z0}+\frac{L_{\theta 0}^{-1}}{2}\sin2\theta_0+\phi_{y0}R_0(\theta_0)=0\ ,$$
$$-\phi_{z0}\cos^2\theta_0+L_{\phi 0}^{-1}\phi_0\cos^2\theta_0+\theta_{y0}R_0(\theta_0)=0\ ,$$
$$\theta_{z1}+\frac{L_{\theta 1}^{-1}}{2}\sin2\theta_1+\phi_{y1}R_1(\theta_1)=0\ ,$$
$$-\phi_{z1}\cos^2\theta_1-L_{\phi 1}^{-1}\phi_1\cos^2\theta_1+\theta_{y1}R_1(\theta_1)=0\ , \tag{12}$$

where $R_j(\theta_j)=\cos^2\theta_j-(1+\kappa_4)[1+\cos2\theta_j]$, with $j=0,1$ at the walls $z_0=0$, $z_1=d$, respectively.

In the PHAN regime, but close to the PHAN-HAN threshold, we look for a solution of the kind

$$\theta(z,y)=\Theta(z)=\epsilon(z,y)\ , \tag{13}$$

where $\epsilon(z,y)$ is a periodic perturbation of the HAN structure described by $\Theta(z)$. To find $\Theta(z)$ we have to solve the equation

$$\Theta_{zz}=0\ , \tag{14}$$

with the following boundary conditions:

$$\Theta_{z0}+\frac{L_{\theta 0}^{-1}}{2}\sin2\Theta_0=0\ ,$$
$$\Theta_{z1}+\frac{L_{\theta 1}^{-1}}{2}\sin2\Theta_1=0\ . \tag{15}$$

Now we go back to the nonlinear system (10), whose perturbed representation is written

$$\epsilon_{zz}+\epsilon_{yy}=0\ ,$$
$$\phi_{zz}+\phi_{yy}-2\Theta_z\phi_z\tan\Theta=0\ , \tag{16}$$

obtained by a simple linearization on ϵ. The perturbed boundary conditions are obtained as

$$\epsilon_{z0}+L_{\theta 0}^{-1}\epsilon_0\cos2\Theta_0+\phi_{y0}R_0(\Theta_0)=0\ ,$$
$$-\phi_{z0}\cos^2\Theta_0+L_{\phi 0}^{-1}\phi_0\cos^2\Theta_0+\epsilon_{y0}R_0(\Theta_0)=0\ ,$$
$$\epsilon_{z1}+L_{\theta 1}^{-1}\epsilon_1\cos2\Theta_1+\phi_{y1}R_1(\Theta_1)=0\ ,$$
$$-\phi_{z1}\cos^2\Theta_1-L_{\phi 1}^{-1}\phi_1\cos^2\Theta_1+\epsilon_{y1}R_1(\Theta_1)=0\ . \tag{17}$$

We now search for a solution of the type [2,4]

$$\epsilon(y,z)=(A\sinh\beta z+B\cosh\beta z)\cos\beta y\ ,$$
$$\phi(y,z)=(C_1e^{k_1z}+C_2e^{k_2z})\sin\beta y\ . \tag{18}$$

We stress the fact that the ϕ differential equation in system (16) has no constant coefficients. To solve the problem, we subdivide the cell into N layers of equal thickness. In each layer we assume the values of Θ equal to the value of the function $\Theta(z)$ calculated in the middle of the layer Θ_i. This is also the case for the derivative $\Theta_z=\Theta_{zi}$. Obviously this procedure is meaningful only if N is large enough.

The second equation of system (16) reads

$$\phi_{zz}^{(i)}+\phi_{yy}^{(i)}+H_i\phi_z^{(i)}=0\ , \tag{19}$$

where $H_i=-2\Theta_{zi}\tan\Theta_i$ for the i layer. Substituting the second equation of system (18) into (19) we found for each layer the values of $k_1^{(i)}$ and $k_2^{(i)}$. What happens to the integration constants $C_1^{(i)}$ and $C_2^{(i)}$, which change from layer to layer? We use them to relate the different solutions $\phi^{(i)}$ at the boundary of the layers $(i)-(i+1)$, imposing continuity to the function ϕ and to its first derivative with respect to z:

$$C_1^{(i)}e^{k_1^{(i)}d_i}+C_2^{(i)}e^{k_2^{(i)}d_i}=C_1^{(i+1)}e^{k_1^{(i+1)}d_i}+C_2^{(i+1)}e^{k_2^{(i+1)}d_i}\ ,$$
$$k_1^{(i)}C_1^{(i)}e^{k_1^{(i)}d_i}+k_2^{(i)}C_2^{(i)}e^{k_2^{(i)}d_i} =k_1^{(i+1)}C_1^{(i+1)}e^{k_1^{(i+1)}d_i}+k_2^{(i+1)}C_2^{(i+1)}e^{k_2^{(i+1)}d_i}\ , \tag{20}$$

where d_i is the distance of the interface between the (i) and the $(i+1)$ layer, from the cell H substrate $z_0=0$.

By the use of a simple linear homogeneous recurrence relation, it is possible to write the coefficient $C_j^{(i)}$ as a function of the first two integration constants $C_1^{(0)},C_2^{(0)}$. Writing the last two coefficients $C_1^{(N)},C_2^{(N)}$ as a function of $C_1^{(0)}$ and $C_2^{(0)}$ and substituting the solutions (15) into the boundary conditions (14), we obtain a linear homo-

geneous system of equations in the arbitrary amplitudes A, B, $C_1^{(0)}$, and $C_2^{(0)}$. Such a system admits a nontrivial solution only if the (4×4) determinant D is equal to zero, providing a dispersion relation. The D elements are given by

$$
\begin{aligned}
a_{11}&=0\ ,\\
a_{12}&=\beta R_0(\Theta_0)\ ,\\
a_{13}&=(k_1^{(0)}-L_{\phi 0}^{-1})\cos^2\Theta_0\ ,\\
a_{14}&=(k_2^{(0)}-L_{\phi 0}^{-1})\cos^2\Theta_0\ ,\\
a_{21}&=\beta L_{\theta 0}\ ,\\
a_{22}&=\cos 2\Theta_0\ ,\\
a_{23}&=L_{\theta 0}\beta R_0(\Theta_0)\ ,\\
a_{24}&=a_{23}\ ,\\
a_{31}&=\beta\sinh(\beta d)R_1(\Theta_1)\ ,\\
a_{32}&=\beta\cosh(\beta d)R_1(\Theta_1)\ ,\\
a_{33}&=\cos^2\Theta_1[(k_1^{(N)}F_N e^{k_1^{(N)}d}+k_2^{(N)}M_N e^{k_2^{(N)}d})\\
&\quad -L_{\phi 1}^{-1}(F_N e^{k_1^{(N)}d}+M_N e^{k_2^{(N)}d})]\ ,\\
a_{34}&=\cos^2\Theta_1[(k_1^{(N)}G_N e^{k_1^{(N)}d}+k_2^{(N)}N_N e^{k_2^{(N)}d})\\
&\quad -L_{\phi 1}^{-1}(G_N e^{k_1^{(N)}d}+N_N e^{k_2^{(N)}d})]\ ,\\
a_{41}&=\sinh(\beta d)\cos 2\Theta_1+L_{\theta 1}\beta\cosh(\beta d)\ ,\\
a_{42}&=\cosh(\beta d)\cos 2\Theta_1+L_{\theta 1}\beta\sinh(\beta d)\ ,\\
a_{43}&=L_{\theta 1}R_1(\Theta_1)(e^{k_1^{(N)}d}F_N+e^{k_2^{(N)}d}M_N)\beta\ ,\\
a_{44}&=L_{\theta 1}R_1(\Theta_1)(e^{k_1^{(N)}d}G_N+e^{k_2^{(N)}d}N_N)\beta\ ,
\end{aligned}
\tag{21}
$$

where F_N, G_N, M_N, and N_N are given by the following recurrence relations:

$$
\begin{aligned}
&F_i=f_iF_{i-1}+g_iM_{i-1}\ ,\quad F_0=f_0\ ,\\
&G_i=f_iG_{i-1}+g_iN_{i-1}\ ,\quad G_0=g_0\ ,\\
&M_i=m_iF_{i-1}+n_iM_{i-1}\ ,\quad M_0=m_0\ ,\\
&N_i=m_iG_{i-1}+m_iN_{i-1}\ ,\quad N_0=n_0\ ,
\end{aligned}
\tag{22}
$$

with

$$
\begin{aligned}
f_i&=\frac{k_2^{(i+1)}-k_1^{(i)}}{k_2^{(i+1)}-k_1^{(i+1)}}\frac{e^{k_1^{(i)}d_i}}{e^{k_1^{(i+1)}d_i}}\ ,\\
g_i&=\frac{k_2^{(i+1)}-k_2^{(i)}}{k_2^{(i+1)}-k_1^{(i+1)}}\frac{e^{k_2^{(i)}d_i}}{e^{k_1^{(i+1)}d_i}}\ ,\\
m_i&=\frac{k_1^{(i)}-k_1^{(i+1)}}{k_2^{(i+1)}-k_1^{(i+1)}}\frac{e^{k_1^{(i)}}}{e^{k_1^{(i+1)}d_i}}\ ,\\
n_i&=\frac{k_2^{(i)}-k_1^{(i+1)}}{k_2^{(i+1)}-k_1^{(i+1)}}\frac{e^{k_2^{(i)}d_i}}{e^{k_1^{(i+1)}d_i}}
\end{aligned}
\tag{23}
$$

coming from the continuity condition of the azimuth ϕ and of its derivative ϕ_z. The dispersion relation $D=0$ provides d as an implicit function of β. In fact we obtain a function $d(\beta,\kappa_4,L_{\phi j},L_{\theta j})$ which for given values of the elastic ratio κ_4 and of the azimuthal- and tilt-extrapolation lengths $L_{\phi j},L_{\theta j}$ provides the correspondence between the possible wave number β of the transverse periodic pattern and the cell thickness d when ϕ is small: this means close to the PHAN-HAN but also to PHAN-P transition. In other words, the vanishing of D given by (16) recovers also the threshold PHAN-P [2]. In particular, such a threshold d_p is the minimum of the curve $d(\beta)$, whereas the threshold PHAN-HAN, d_a, corresponds to the maximum of the same function, provided both situations correspond to minima of the cell reduced free energy G. In Fig. 2 the thresholds d_p,d_a are reported vs the elastic ratio κ_4, for different values of the tilt anchoring strengths $L_{\theta j}$, when the azimuthal anchoring is negligible ($L_{\phi j}=\infty$). Note that all lengths are normalized by the asymptotic HAN-P threshold $d_a^{\rm as}\equiv L_{\theta 0}-L_{\theta 1}$ [12].

III. EXPERIMENT

Our experiments have been made using the liquid crystal pentylcyanobiphenyl, 5CB (purchased from EM Industries, Inc.), which exhibits the nematic phase at room temperature. All sample preparations and measurements were performed at room temperature. To provide a hybrid aligned film with zero anchoring in the horizontal plane, a small drop (1–10 mg) of the nematic has been deposited on an isotropic liquid substrate, which does not dissolve the liquid crystal. As a substrate we have used glycerine, providing the tangential orientation of the

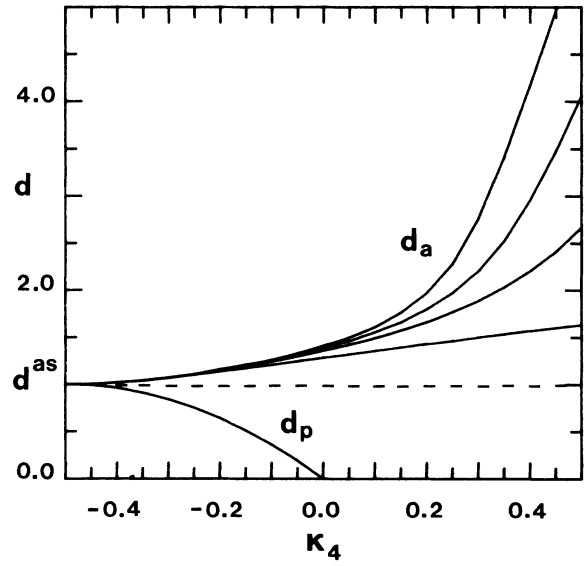

FIG. 2. PHAN-P threshold d_p and PHAN-HAN threshold d_a as function of the saddle-splay–to–bulk elastic ratio $\kappa_4\equiv K_{24}/K$ for different values of the reduced tilt anchoring strengths $L_{\theta 0}/d_s^{\rm as},L_{\theta 1}/d_a^{\rm as}$, normalized to the asymptotic threshold HAN-P $d_a^{\rm as}=L_{\theta 0}-L_{\theta 1}$, at the H and P walls, respectively, for no twist anchoring ($L_{\phi 0}=L_{\phi 1}=\infty$).

director **n** at the lower film boundary, which acts as a P wall. Such a feature has been checked up independently by suspending small liquid crystalline droplets in a glycerine matrix: these drops display bipolar structure which implies the tangential boundary conditions [18,19]. The upper boundary of the film has been left free; thus the director orientation was nearly normal to it, providing an H wall (see Fig. 3). The box with glycerine and nematic layers has been enclosed in order to minimize the contamination. Because of the nonzero contact angle, the spread nematic drops have a nonflat profile. The average thickness d of the liquid crystalline film has been estimated by the measurements of the drop weight and of the surface area of the spread film (typically 20–50 cm^2).

It was found that the HAN configuration, which is uniformly oriented in the horizontal plane, is unstable with respect to the appearance of the periodic domain pattern (PHAN) when the film thickness d is smaller than a first critical value d_a. For the 5CB-glycerine interface $d_a = 0.4 \pm 0.1$ μm. On the other hand, for d smaller than a second critical value d_p, the unidirectional (at least in the horizontal plane) P structure is found to be more stable with respect to PHAN. In our case of nonflat droplets d_p was estimated to be less than 0.15 μm. The observed domain textures are shown in Figs. 4 and 5. A periodic stripe pattern appears in sufficiently thin films; the periodicity of the structure strongly depends on the film thickness and decreases as one moves towards the drop edge. If the nematic drop is thin, then the spread nematic layer has thickness $d < d_a$ everywhere. This is the case of Fig. 4, where the drop shows the stripe pattern everywhere except a narrow periphery region with almost unidirectional orientation along the normal to the drop border (x axis). On the other hand, if the nematic drop is thick enough (Fig. 5) the central part has $d > d_a$ and the domain structure appears only at the periphery where $d_p < d < d_a$. The domains are elongated along the normal x to the film edge. The domain textures depend on the orientation of the crossed polarizers of a microscope with respect to x. To describe these textures it is convenient to use the notation n_{xy} for the horizontal component of the director field at the lower boundary of the film, i.e., at the P wall $z_1 = d$. If one of the polarizers is oriented along the x axis, the domains appear as bright regions interrupted by thin dark lines of extinction (see Fig. 6). Alternatively, the thicker neighboring part of the film (where $d > d_a$) looks like a dark field due to the uniform alignment of n_{xy} along the x axis. When one rotates the sample between the crossed polarizers, the dark thin lines in the domain region move and extend, and the texture transforms into an alternation of broad dark and light stripes (Fig. 6). Such a behavior is similar to that observed by Livolant and Bouligand for columnar phases of some bipolymers [DNA and poly γ-benzyl L-glutamate (PBLG)] with sinuous undulation [20]. However, as shown by the use of a quartz wedge, the geometry of n_{xy} is different (see Fig. 6).

FIG. 4. Small 5CB drop, viewed through crossed polarizers. The PHAN-P line, where the cell thickness is d_p, is close to the boundary of the drop. Bar length is 125 μm.

Each domain consists of two parallel subdomains with equal thickness but opposite inclination on n_{xy} with respect to the x axis. At the boundary of the subdomains n_{xy} is parallel to the x axis and thus coincident with n_{xy} in the neighboring uniform part of the film. The angle α of the n_{xy} inclination compared to the x axis grows from $\alpha = 0$ at the subdomain boundary to some maximal value $\alpha = \alpha_M$ at the central part of the subdomain. As the thickness of the film decreases, one observes (i) reducing of the domain periodicity λ; (ii) appearance of dislocations with the Burgers vector equal to λ, and (iii) nucleation of new domain generation with smaller periodicity and with new preferable orientation x', which is tilted with respect to the x axis (see Fig. 7). Sometimes the

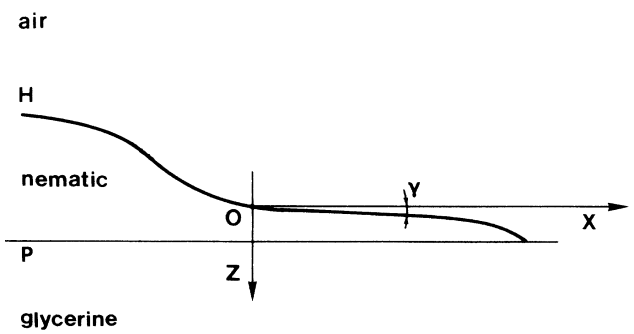

FIG. 3. Crude representation of the spreading of the nematic droplet profile.

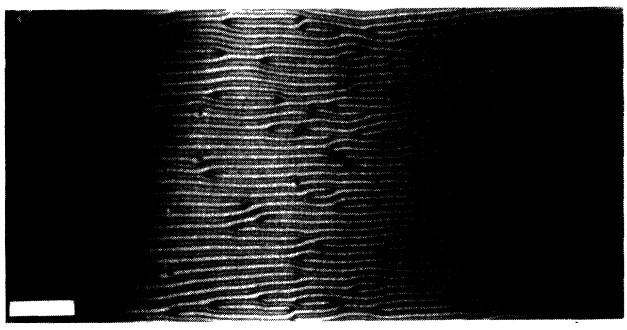

FIG. 5. Precursor of a big 5CB drop, viewed through crossed polarizers. The PHAN-HAN line, where the cell thickness is d_a, is towards the drop center. Bar length is 150 μm.

third domain generation as well as square lattices of point defects are observed. The decrease of the domain periodicity λ with the film thickness d might be illustrated by Fig. 8, where λ is plotted as a function of the distance x between the threshold line, which corresponds to $d=d_a$,

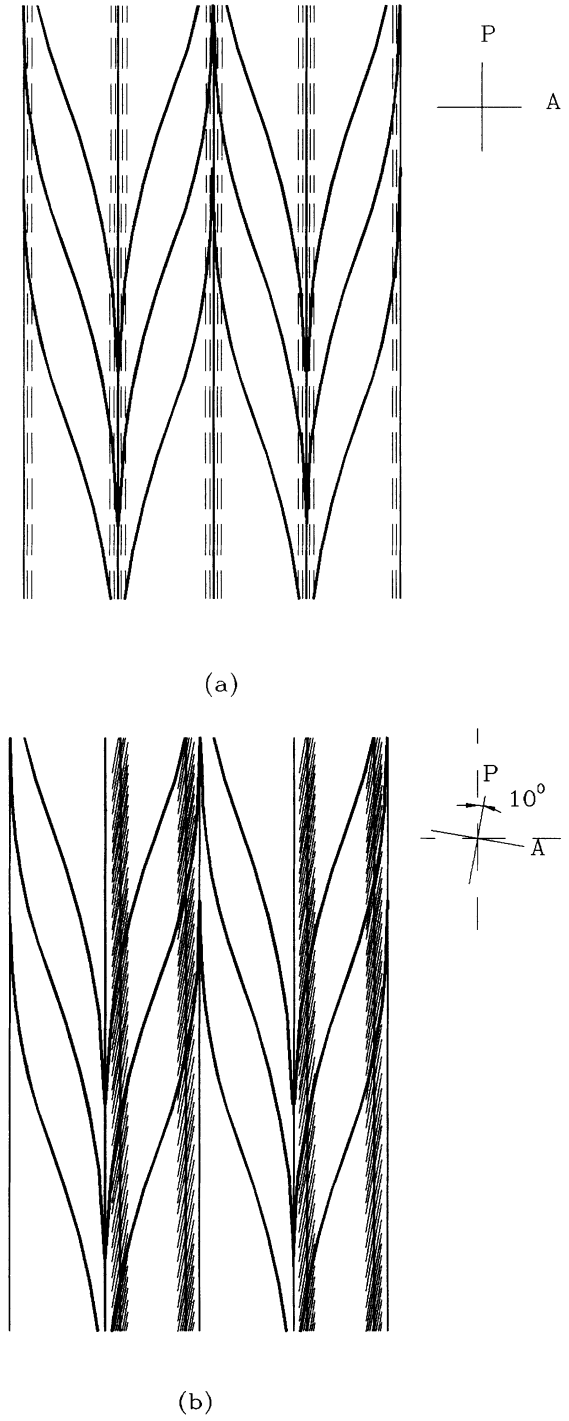

FIG. 6. Periodic domain pattern of the nematic film: n_{xy} distribution and extinction bands (dashed areas) for different orientations of the crossed polarizer. Extinction bands occur in those places of the texture where n_{xy} coincides with direction of polarization either of the polarizer or of the analyzer.

FIG. 7. The nucleation of the secondary domain generation with common direction x' which is inclined with respect to x: texture. Bar length is 200 μm.

and the point of measurement. It is important to note that in principle one can reconstruct the precursor shape of the drop by the measurements of $\lambda(x)$, if the dependency $\lambda(d)$ is known. For example, if λ were a linear function of d, then the precursor shape would be represented just by the profile $\lambda(x)$.

As shown in [21] and briefly discussed below, the nonflat profile of 5CB droplets deposited directly onto the glycerine substrate results in a specific "geometrical" azimuthal anchoring. The azimuthal anchoring in accordance with the considerations given above affects the parameters of the periodic pattern and thus leads to difficulties in the determination of K_{24}. To avoid the problem we have prepared another type of sample. The liquid crystal was dissolved in hexane. The solution was deposited onto the glycerine substrate and the solvent was evaporated in a clean environment. The resulting 5CB films show uniform thickness and the periodicity of the PHAN pattern does not change much from point to

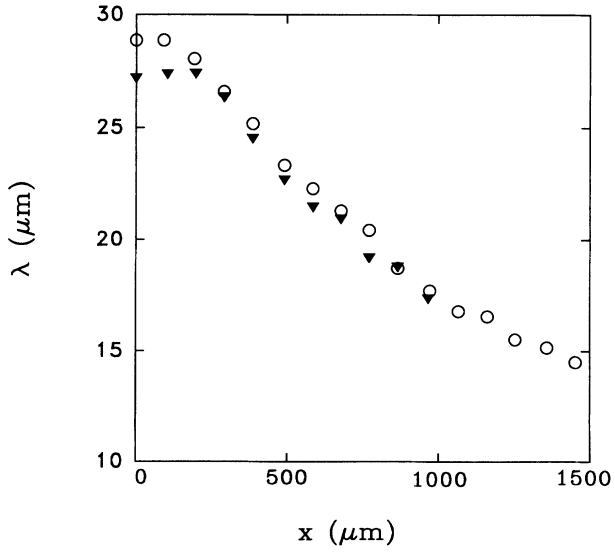

FIG. 8. PHAN pattern wavelength as function of the x distance from the HAN-PHAN threshold in big droplets: experimental data on two different samples.

point. For this type of film and for a temperature of 24.5 °C the PHAN structure occurs starting with $d_a = 0.48 \pm 0.05$ μm and $\lambda = 180$ μm. The thinnest film possessing PHAN structure we were able to identify had $d = 0.02 \pm 0.01$ μm and $\lambda = 2$ μm. Films thinner than 0.02 μm still possess birefringence but it is difficult to distinguish a periodic pattern.

IV. DISCUSSION

A. Degenerated torsional anchoring

Due to the isotropic nature of both the surrounding media, glycerine and air, the boundary conditions for **n** were degenerated in the film plane. Really, all the horizontal orientations of the nematic lines which keep the same polar angles have the same energy. This means that in the flat film the torsional extrapolation lengths $L_{\phi 0}$ at the air side and $L_{\phi 1}$ at the glycerine boundary are infinitely large. Thus the boundary conditions (17) and consequently the dispersion relation $D = 0$—see (21)—become simpler, and it is easy to estimate the saddle-splay elastic constant K_{24}. Let us assume that the tilt anchoring strength $L_{\theta 0}$ at the upper side is $W_{\theta\sigma} \approx 1 \times 10^{-5}$ N/m. Since for 5CB we have $K \approx 7$ pN, $L_{\theta 0} \approx 0.7$ μm is obtained. From our experimental data ($d_p \leq 0.02$ μm, $d_a \approx 0.48$ μm), we derive from the dispersion relation $D = 0$, in the first case a numerical relation κ_4 vs $L_{\theta 1}$ providing d_a is approximatively equal to the experimental value, and in the second case another numerical relation κ_4 vs $L_{\theta 1}$, providing d_p [see Figs. 9(a) and 9(b)]. By simple inspection of this figure, we can see that d_a determines the values of $L_{\theta 1} = 0.35$ and that $d_p \leq 0.02$ gives $-0.012 \leq \kappa_4 < 0$. The symmetry of the PHAN allows also the second estimate $0.988 < \kappa_4 < 1.0$, since the values $+|1-2\kappa_4|$ and $-|1-2\kappa_4|$ correspond to the same structure. Note that κ_4 is deeply affected by the value of d_p.

Our estimate of κ_4 is consistent with the NMR measurements in confined geometry by Allender, Crawford, and Doane [26], who obtained for 5CB, according to our notations, $1 + \kappa_4 = 1.0 \pm 0.6$, i.e., $\kappa_4 = -0.6 - 0.6$.

In order to recover the experimental results for the droplets with nonflat boundaries, it is necessary to take into account a possible breaking of the azimuthal anchoring degeneracy at the upper surface, due to the so-called geometrical anchoring [4,21]. Really, for a nematic film with parallel upper and lower surfaces, all the horizontal orientations of the nematic lines which keep the same polar angle θ at the film surfaces but different azimuthal angles ϕ have the same energy. However, this physical degeneracy can be removed by the geometrical factor, namely, by the boundary curvature and the gradients of the film thickness d. Let us consider this point in greater detail.

B. Geometrical anchoring at the inclined air-nematic interface

In experiments with nematic drop placed on the glycerine surface we deal with the so-called wetting regime [22], when the liquid crystal forms a film of some profile $d(r)$. The dependency of the film thickness vs the distance **r** between the film center and the point of observation is very complicated to describe and measure even for the simplest case of a usual liquid drop spreading on a rigid surface, see, e.g., the review article by de Gennes [23]. Using the liquid crystal instead of a simple liquid and a fluid (glycerine) substrate instead of a rigid one, the situation is not improved. However, one could expect that the nematic film will also consist of two different parts: the central macroscopic part, which is spread by the Laplace pressure due to the curved interfaces and a thin precursor part of submicrometric thickness, which extends ahead of the spreading drop and whose thickness is governed by long-range forces, see, e.g., [24]. The single point of our interest here is the evident fact that the inclination angle γ of the upper nematic interface with respect to the lower one strongly depends on the distance r between the film center and the point of measurement: γ is exactly 0 for $r = 0$, approaches zero in the precursor tail, and takes some maximum value γ_M in the intermediate region between the macroscopic and the microscopic parts of the film (see Fig. 3). The question is—how will the director line be oriented in this intermediate region? For the sake of simplicity let us assume that (i) the lower

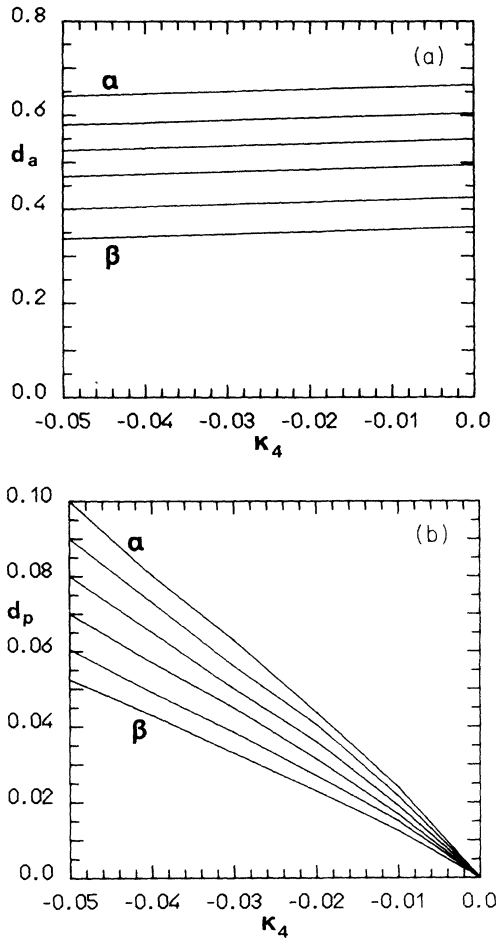

FIG. 9. Threshold thickness for the HAN-PHAN (a) and for the *P*-PHAN (b) transition as a function of κ_4 for $L_{\theta 0} = 0.7$ μm and $L_{\theta 1}$ ranging, with a step of 0.05 μm, from 0.20 (curve α) to 0.45 μm (curve β).

interface is flat and (ii) the polar anchoring is strong everywhere, thus the angles θ_0 and θ_1 between $\mathbf{n}$ and the upper and the lower surfaces, respectively, are constant. Due to the isotropic nature of the ambient media, the set of the easy directions of $\mathbf{n}$ at both surfaces is represented by two cones of revolution with symmetry axis coincident with the normals, ν_0,ν_1, and with cone angle $\pi/2-\theta_0,\pi/2-\theta_1$, respectively—see Fig. 10(a). In the so-called one-constant approximation for the density of the elastic energy, Eq. (1) in the absence of saddle-splay gives

$$f=\frac{K}{2}[(\mathrm{div}\mathbf{n})^2+(\mathrm{curl}\mathbf{n})^2] \ . \tag{1'}$$

As shown in Ref. [25], the tilt angle $\theta(z)$ is a linear function of the vertical coordinate $\mathbf{z}$, $\theta(z)=\theta_0-\alpha z$, where $\alpha=(\theta_0-\theta_1)/d$ and $z=0$ at the upper surface. For the case of parallel interfaces the director distribution reads

$$\begin{aligned} n_x &= 0 \ , \\ n_y &= \sin(\theta_0-\alpha z) \ , \\ n_z &= \cos(\theta_0-\alpha z) \ , \end{aligned} \tag{24}$$

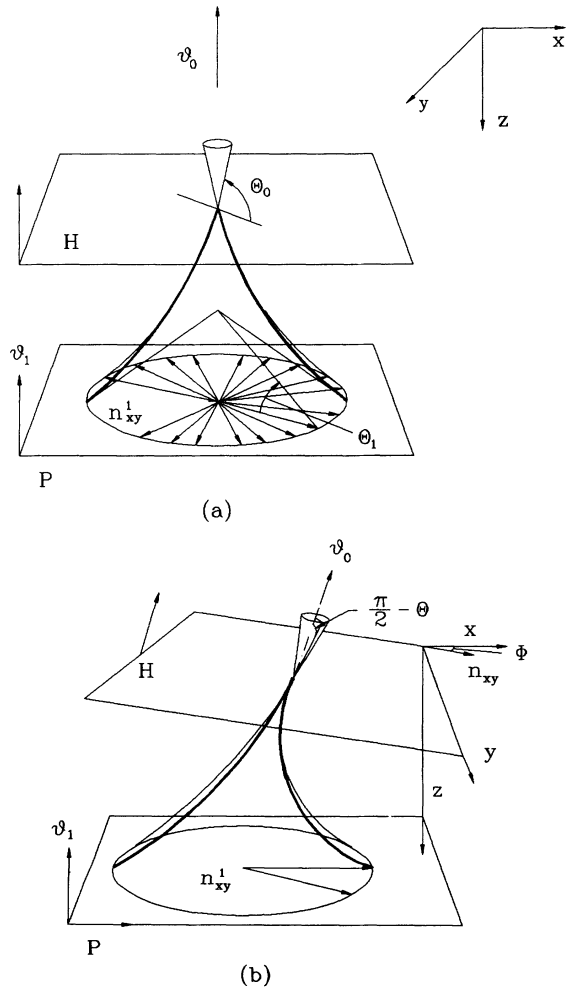

FIG. 10. The physical degeneracy of the azimuthal orientation in the HAN film (a) is removed by the inclination of the film surface (b).

and the curvature elastic energy per unit surface of the film is $F=Kd\alpha^2/2$. However, with nonzero tilt γ of the upper surface [Fig. 10(b)] the new curvature α' is determined not only by the polar angles θ_0,θ_1, but also by γ and the azimuthal angle ϕ, which, as already stated, is measured in the horizontal plane between the direction of the thickness gradient and the projection of $\mathbf{n}$; for small tilts we have

$$\alpha' \cong (\theta_0-\theta_1-\gamma\cos\phi)/d \ . \tag{25}$$

Taking into account in the distribution (24) the azimuthal dependency of the curvature (25), one obtains from Eq. (1') the azimuth-dependent elastic energy of the film with nonzero tilt of the upper surface: $F'=F+W_g$, where the geometrical anchoring is

$$W_g=\frac{K}{d}\left[\frac{\gamma^2\cos^2\phi}{2}-(\theta_0-\theta_1)\gamma\cos\phi\right] . \tag{26}$$

Thus the physical degeneracy of the azimuthal director orientation turns out to be removed when the film surfaces are mutually inclined.

The profile of the geometrical anchoring energy strongly depends on the ratio $\rho=(\theta_0-\theta_1)/\gamma$ (see Fig. 11), and results in an interesting behavior of the elastic energy. As one deduces from this figure, the equilibrium easy direction ϕ_0 for the nematic lines which is imposed by the "geometrical" anchoring varies from $\phi_0=\pm\pi/2$ for $\rho=0$ (similar boundary conditions at both surfaces) to $\phi_0=0$ for $\rho>1$ through some intermediate values $0<|\phi_0|<\pi/2$ for $0<\rho<1$.

One should keep in mind that in the real situation the polar anchoring is finite and the values θ_0 and θ_1 depend on the film thickness d in such a way that $\theta_0-\theta_1$ is smaller in the thinner part. Thus ρ and the easy direction will vary with $\mathbf{r}$ in a very complicated way due to the nonmonotonic dependency $\gamma(r)$ and the monotonic dependency $(\theta_0-\theta_1)$ on d. However, for the thick part with $(\theta_0-\theta_1)\approx 70°-80°$, one should expect that $\rho>1$ and the easy direction is coincident with the thickness gradient,

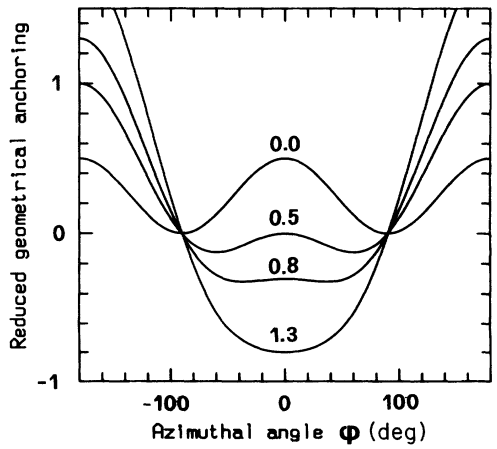

FIG. 11. Reduced geometrical anchoring $W_g d/K\gamma^2$ vs azimuthal orientation ϕ for different values of ratio $\rho=(\theta_0-\theta_1)/\gamma$ ranging from 0 to 1.3.

i.e., with the horizontal axis x normal to the film edge. This corresponds to the experimental observation: n_{xy} and the x axis are parallel in the vicinity of the critical thickness d_a. The geometrical azimuthal anchoring strength has been previously estimated for $d \sim d_a$ to be $L_{\phi 0} \approx 10-100\ \mu$m [4].

As we can see from our experimental results, the threshold d_p measured for nonflat droplets ($d_p \lesssim 0.15\ \mu$m) is larger than d_p measured for the flat films ($d_p \lesssim 0.02\ \mu$m). This difference is a natural result of the nonzero geometrical anchoring in the case of a nonflat profile. Taking for the values of $L_{\theta 1}$ and κ_4 the values obtained in the flat geometry, and analyzing the threshold d_p as a function of the geometrical anchoring $L_{\phi 0}$ (that is unknown close to d_p), we estimate the last parameter to be 10 μm. In this case the value of d_p is greater for nonflat droplets than for flat films in accordance with experiment.

V. CONCLUSION

The appearance of a PHAN configuration of splay type (due to the tilt anchoring strengths) was considered, against the usual HAN structure. For the sake of simplicity, the bulk elastic isotropy was assumed. The behavior of the PHAN-HAN threshold d_a and of the recovered PHAN-P threshold d_p were predicted theoretically vs the surface-to-bulk elastic ratio κ_4 and the tilt and azimuthal anchoring strengths.

Experiments were performed on films and droplets of 5CB wetting a glycerine substrate. The PHAN pattern, appearing in both cases, allows a measurement of $d(\beta)$, providing the critical values. By assuming $L_{\theta 0}$ at the 5CB-air interface at room temperature to be kept at the same value (2 μm) as obtained in Ref. [9] for the same experimental conditions, two crossed best fits at both thresholds provide an estimate of $L_{\theta 1}$ at the 5CB-glycerine interface and of the saddle-splay–to–bulk ratio $\kappa_4 \equiv K_{24}/K$. The latter value was found to be $\kappa_4 = -0.012 - -0.0$, consistent with the only measurement of κ_4 in the same material reported in the literature [26]. Furthermore, second and third domain generations of PHAN as well as square lattices of point defects were observed: a theoretical model explaining such a phenomenon (and the influence of K_{24}) is almost complete.

Moreover, experiments with 5CB cells in the presence of a magnetic field either preventing or favoring the PHAN configuration are under way and will be published elsewhere.

ACKNOWLEDGMENT

One of us (O.D.L.) thanks the National Science Foundation for support [Grant No. DMR89-20147 (ALCOM)].

[1] A. Sparavigna, L. Komitov, B. Stebler, and A. Strigazzi, Mol. Cryst. Liq. Cryst. **207**, 265 (1991).
[2] A. Sparavigna and A. Strigazzi, Mol. Cryst. Liq. Cryst. **221**, 109 (1992).
[3] A. Sparavigna, L. Komitov, and A. Strigazzi, Mol. Cryst. Liq. Cryst. **212**, 289 (1992).
[4] A. Sparavigna, L. Komitov, O. D. Lavrentovich, and A. Strigazzi, J. Phys. (Paris) II **2**, 1881 (1992).
[5] S. Matsumoto, M. Kawamoto, and K. Mizunaya, J. Appl. Phys. **47**, 3842 (1976).
[6] Yu. P. Bobylev and S. A. Pikin, Zh. Eksp. Teor. Fiz. **72**, 369 (1977) [Sov. Phys. JETP **45**, 195 (1977)].
[7] F. Lonberg and R. B. Meyer, Phys. Rev. Lett. **55**, 718 (1985).
[8] E. Miraldi, C. Oldano, and A. Strigazzi, Phys. Rev. A **34**, 4348 (1986).
[9] O. D. Lavrentovich and V. M. Pergamenshchik, Mol. Cryst. Liq. Cryst. **179**, 125 (1990).
[10] V. M. Pergamenshchik, Phys. Rev. E **47**, 1881 (1993).
[11] A. Rapini and M. Papoular, J. Phys. (Paris) Colloq. **30**, CA-54 (1969).
[12] G. Barbero and R. Barberi, J. Phys. (Paris) **44**, 609 (1983).
[13] J. Nehring and A. Saupe, J. Chem. Phys. **54**, 337 (1971); **56**, 5527 (1972).
[14] G. Barbero, A. Sparavigna, and A. Strigazzi, Nuovo Cimento D **12**, 1259 (1990).
[15] P. G. de Gennes, *The Physics of Liquid Crystals* (Clarendon, Oxford, 1974).
[16] M. Kléman, *Points, Lignes, Parois* (Ed. Physique, Paris, 1977).
[17] V. Smirnov, *Cours des Mathématiques Supérieures* (Mir, Moscow, 1975), Vol. IV.
[18] G. E. Volovik and O. D. Lavrentovich, Zh. Eksp. Teor. Fiz. **85**, 1997 (1983) [Sov. Phys. JETP **58**, 1159 (1983)].
[19] M. V. Kurik and O. D. Lavrentovich, Usp. Fiz. Nauk. **154**, 381 (1988) [Sov. Phys. Usp. **31**, 196 (1988)].
[20] F. Livolant and Y. Bouligand, J. Phys. (Paris) **47**, 1813 (1986).
[21] O. D. Lavrentovich, Phys. Rev. A **46**, 722 (1992).
[22] B. Jérome, Mol. Cryst. Liq. Cryst. **212**, 21 (1992).
[23] P. G. de Gennes, Rev. Mod. Phys. **57**, 827 (1985).
[24] J. Daillant, J. J. Benattar, and L. Leger, Phys. Rev. A **41**, 1963 (1990).
[25] G. Barbero and A. Strigazzi, Fizika **13**, 85 (1981).
[26] D. W. Allender, G. P. Crawford, and J. W. Doane, Phys. Rev. Lett. **67**, 1442 (1991).

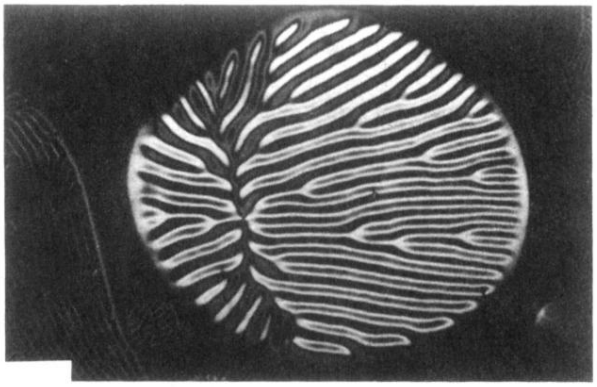

FIG. 4. Small 5CB drop, viewed through crossed polarizers. The PHAN-*P* line, where the cell thickness is d_p, is close to the boundary of the drop. Bar length is 125 μm.

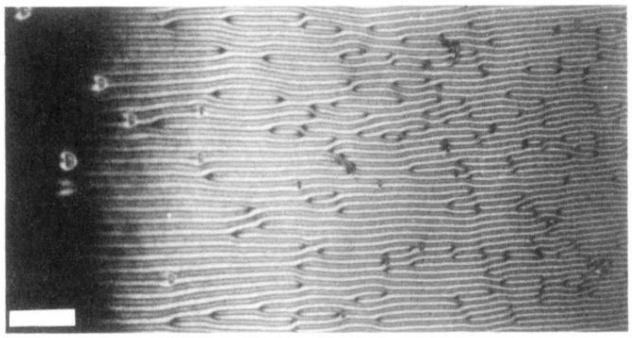

FIG. 5. Precursor of a big 5CB drop, viewed through crossed polarizers. The PHAN-HAN line, where the cell thickness is d_a, is towards the drop center. Bar length is 150 μm.

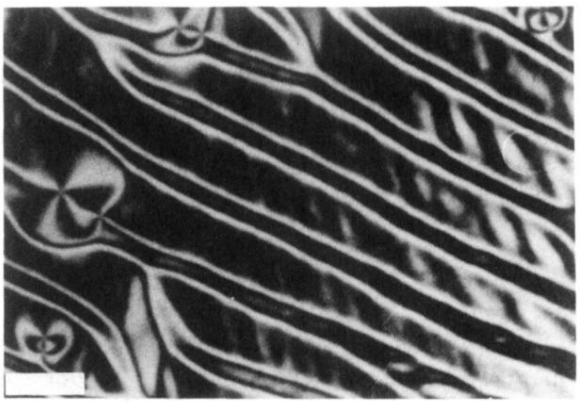

FIG. 7. The nucleation of the secondary domain generation with common direction x' which is inclined with respect to x: texture. Bar length is 200 μm.